

Relative dispersion in generalized two-dimensional turbulence

Alexis Foussard^{1,2}, Stefano Berti³, Xavier Perrot¹ and Guillaume Lapeyre^{1,†}

¹LMD/IPSL, CNRS/ENS, 24 rue Lhomond, 75005 Paris, France

²Ecole des Ponts Paris Tech, Cité Descartes, 6–8 Avenue Blaise Pascal, 77455 Champs-sur-Marne, France

³Université de Lille, CNRS, FRE 3723, Laboratoire de Mécanique de Lille, 59000 Lille, France

(Received 20 July 2016; revised 28 March 2017; accepted 14 April 2017)

The statistical properties of turbulent fluids depend on how local the energy transfers among scales are, i.e. whether the energy transfer at some given scale is due to the eddies at that particular scale, or to eddies at larger (non-local) scale. This locality in the energy transfers may have consequences for the relative dispersion of passive particles. In this paper, we consider a class of generalized two-dimensional flows (produced by the so-called α -turbulence models), theoretically possessing different properties in terms of locality of energy transfers. It encompasses the standard barotropic quasi-geostrophic (QG) and the surface quasi-geostrophic (SQG) models as limiting cases. The relative dispersion statistics are examined, both as a function of time and as a function of scale, and compared to predictions based on phenomenological arguments assuming the locality of the cascade. We find that the dispersion statistics follow the predicted values from local theories, as long as the parameter α is small enough (dynamics close to that of the SQG model), for sufficiently small initial pair separations. In contrast, non-local dispersion is observed for the QG model, a robust result when looking at relative displacement probability distributions. However, we point out that spectral energy transfers do have a non-local contribution for models with different values of α , including the SQG case. This indicates that locality/non-locality of the turbulent cascade may not always imply locality/non-locality in the relative dispersion of particles and that the self-similar nature of the turbulent cascade is more appropriate for determining the relative dispersion locality.

Key words: geophysical and geological flows, geostrophic turbulence, mixing and dispersion

1. Introduction

The spreading process of an ensemble of particles advected by a turbulent fluid depends on the stirring properties of the velocity field, which can be quantified by its strain rate (Batchelor 1952*b*; Garrett 1983) and its Lagrangian derivatives (Hua, McWilliams & Klein 1998; Klein, Hua & Lapeyre 2000). There are intricate relations between the cascades of two-dimensional (2D) or three-dimensional (3D) turbulence

† Email address for correspondence: glapeyre@lmd.ens.fr

and the dispersion of passive particles (see e.g. Falkovich *et al.* 2001; Sawford 2001; Salazar & Collins 2009). In 2D turbulence, relative enstrophy is transferred towards small scales through a (marginally) non-local turbulent cascade for which straining processes at small scales are driven by large-scale eddies (Ohkitani 1990; Oetzel & Vallis 1997). In contrast, kinetic energy is transferred towards large scales through a local turbulent cascade (Kraichnan 1967; Boffetta & Ecke 2012). As a result, one can expect that the large-scale strain will dominate the dispersion properties in the range of scales corresponding to the direct enstrophy cascade, while the dispersion will be affected by local scales in the inverse cascade range (Kowalski & Peskins 1981).

Using self-similarity arguments, Morel & Larcheveque (1974) and Bennett (1984) proposed a relation between the slope of the kinetic energy spectrum and the laws of relative dispersion between particle pairs. They distinguished two dynamical regimes. In the first one, qualified as ‘local’, the dispersion laws at a particular length scale l depend only on flow statistics at that length scale. This is the case for kinetic energy spectra shallower than k^{-3} (with k the horizontal wavenumber). For a kinetic energy spectrum in $k^{-5/3}$, based on self-similarity arguments of the turbulent cascade, one would obtain the Richardson dispersion law $y^2 \propto t^3$, where y is the distance between a pair of particles. On the other hand, in the second ‘non-local’ regime, corresponding to kinetic energy spectra steeper than k^{-3} , the dispersion laws should depend on the largest and dominant scales of the fluid (Bennett 1984). In this case, y^2 would grow exponentially in time.

This distinction is discussed in a geophysical context by Özgökmen *et al.* (2012), who examined the dispersion of particles in oceanic flows with more or less vigorous submesoscales (scales below the Rossby radius of deformation). For weakly intensified submesoscales, whose kinetic energy spectrum is steeper than k^{-3} , relative dispersion is found to be fairly scale-independent. In that situation, relative dispersion characteristics depend not on the dispersion scale but on much larger ones. For more intensified submesoscales, the kinetic energy spectrum is shallower than k^{-3} and the dispersion laws are a function of the dispersion scale (Özgökmen *et al.* 2012). Berti & Lapeyre (2014) obtained a different result in a situation where the kinetic energy spectrum is close to k^{-2} , for which dispersion could be expected to be local. They observed that the large-scale stirring was responsible for the formation of a considerable amount of submesoscales, even if small-scale eddies determined the spatial distribution of a tracer at very small scales (Berti & Lapeyre 2014). This suggests that the locality of the stirring or dispersion might have a non-obvious correspondence with energy spectra in 2D turbulent fluids. This was also noted by Nicolleau & Yu (2004), who examined particle pair dispersion statistics in 3D kinematic simulations, focusing on the dependence on the kinetic energy spectral slope. However, this last result should be taken with some caution, as kinematic simulations do not take into account the sweeping of small-scale eddies by large-scale ones (Thomson & Devenish 2005).

Here a caveat has to be given since turbulence is characterized in itself not by kinetic energy spectra, but by energy cascades between scales. Self-similarity arguments can then be given, and allow one to relate the dispersion laws to the local flux of energy and to the local length scale (see e.g. Batchelor 1950). In general, self-similarity theories based on the kinetic energy spectral slope give the same result as theories based on the basic characteristics of the turbulence (the existence of an inertial range and of a local energy flux). The reason is that the kinetic energy spectral slope is also a by-product of self-similarity arguments on the energy cascade.

Several studies have been devoted to the analysis of relative dispersion from experimental data and numerical simulations, focusing on the correspondence between

dispersion laws and energy spectra. In the oceanographic context, numerous studies have looked for scaling laws for dispersion of floats or surface drifters. In particular there was some evidence of a t^3 power law in the North Atlantic (LaCasce & Bower 2000; Ollitrault, Gabillet & Colin de Verdière 2005) and in the Gulf of Mexico (LaCasce & Ohlmann 2003). The existence of an exponential regime that would suggest a direct enstrophy cascade is more delicate (LaCasce & Ohlmann 2003; Ollitrault *et al.* 2005; Koszalka, LaCasce & Orvik 2009). More generally, Lumpkin & Elipot (2010) discuss local and non-local dispersion regimes in different sets of surface drifters data in the North Atlantic Ocean through different Lagrangian indicators. In particular, they find a regime of enhanced relative dispersion at small scales that would suggest a kinetic energy spectrum as shallow as k^{-2} at submesoscales. Such a regime has also been observed in a series of other recent works dealing with surface drifters data in different regions of the world oceans (Ollitrault *et al.* 2005; Berti *et al.* 2011; Schroeder *et al.* 2012). A detailed review of analogous results can be found in LaCasce (2008). Concerning atmospheric flows, relative dispersion characteristics were examined by different authors using trajectories of pressure balloons in the stratosphere (e.g. Lin 1972; Morel & Larcheveque 1974; Er-El & Peskin 1981) to assess the possibility of a direct enstrophy cascade in the atmosphere. Owing to the limited availability of data and the anisotropy of the flow, results were not completely conclusive when examining dispersion as a function of time. Lacorata *et al.* (2004) revisited the data of Morel & Larcheveque (1974) using finite-size Lyapunov exponents (Aurell *et al.* 1997) and found a dispersion behaviour compatible with a $k^{-5/3}$ kinetic energy spectrum. Using trajectories from a Lagrangian dispersion model employing reanalysis wind fields, Graff, Guttu & LaCasce (2015) found an exponential growth consistent with non-local dispersion in the upper troposphere.

Relative dispersion in numerical simulations of 2D turbulence has been investigated both in the inverse energy cascade and in the direct enstrophy cascade. In the inertial range of the inverse energy cascade, it was found that relative dispersion nearly followed Richardson's law (Babiano *et al.* 1990; Boffetta & Celani 2000; Poje *et al.* 2010). This is also the case for laboratory experiments reported in Jullien, Paret & Tabeling (1999). In the inertial range of the direct enstrophy cascade, the exponential law was more difficult to observe in direct numerical simulations (Kowalski & Peskins 1981; Babiano *et al.* 1990) and in experiments (Jullien 2003). Laboratory experimental measurements based on a 2D fluid driven by Faraday waves allowed the observation of Richardson's regime (Von Kameke *et al.* 2011) in the inverse energy cascade. For electromagnetically forced fluids, Rivera & Ecke (2005) observed doubling-time statistics (Aurell *et al.* 1997) consistent with the exponential law predicted in the direct enstrophy range and a power-law regime in the inverse energy cascade. Many of these studies found difficulties in observing a clear relation between the kinetic energy spectral slope and relative dispersion. One reason invoked is the dependence of scaling laws on the initial particle pair separation. This issue was discussed in detail by Babiano *et al.* (1990) and Boffetta & Sokolov (2002) with 2D direct numerical simulations, and by Nicolleau & Yu (2004) using kinematic simulations in three dimensions and Ollitrault *et al.* (2005) with floats in the ocean. Other reasons may be invoked, such as the presence of coherent vortices (Jullien 2003).

The subject of the present paper is to study a class of 2D flows, the so-called α -turbulence models (Pierrehumbert, Held & Swanson 1994), which share the common feature of exhibiting both direct and inverse cascades of an active tracer. One characteristic of these models is that the kinetic energy spectral slope depends on the parameter α (Watanabe & Iwayama 2004) and that energy fluxes are supposed to

be driven by local scales for small α and non-local scales for large α (Pierrehumbert *et al.* 1994). Hence, one can try to see if there is some relation between the non-locality of the spectral energy transfers and the non-locality of particle dispersion. Two important models of geophysical interest belong to this class of α -turbulence: the barotropic quasi-geostrophic (QGBT) model and the surface quasi-geostrophic (SQG) model (Held *et al.* 1995; Lapeyre 2017). On the one hand, in the QGBT model, relative vorticity is conserved along the geostrophic flow; on the other hand, in the SQG model, surface temperature is conserved (along the geostrophic flow) and potential vorticity is constant within the bulk of the fluid. Both models are relevant, in particular, for the dynamics of oceanic flows with meso- and submesoscale motions, as the SQG model resembles what occurs at the ocean surface while the QGBT model resembles what occurs in the interior (Klein *et al.* 2011). Phenomenologically, QGBT turbulence (respectively, SQG turbulence) is related to kinetic energy spectra in k^{-3} (respectively $k^{-5/3}$) in the direct cascade of enstrophy (respectively temperature variance).

The remainder of this paper is organized as follows. After a short review of the phenomenology of the relation between 2D turbulence and relative dispersion (§ 2), we present the numerical model that is used in our study (§ 3). Then § 4 is dedicated to the properties of the generalized 2D turbulent flows, while § 5 concerns the statistics of relative dispersion in α -turbulence. Conclusions are drawn in § 6.

2. Theory

2.1. Models of two-dimensional turbulence

In the QGBT model, relative vorticity ζ is a Lagrangian conserved tracer advected by the geostrophic flow,

$$\frac{\partial \zeta}{\partial t} + \mathbf{u} \cdot \nabla \zeta = 0, \quad (2.1)$$

where $u = -\partial \psi / \partial y$ and $v = \partial \psi / \partial x$ are the two components of the incompressible velocity field \mathbf{u} , ψ is the streamfunction and $\zeta = \partial v / \partial x - \partial u / \partial y = \nabla^2 \psi$. In horizontal Fourier space, we can write this last equation as

$$\widehat{\zeta} = -k^2 \widehat{\psi}, \quad (2.2)$$

where the hat stands for the Fourier transform and k is the horizontal wavenumber modulus.

Another classical quasi-geostrophic (QG) model is the SQG model, whose potential vorticity is uniform throughout the interior of the fluid (Held *et al.* 1995; Lapeyre 2017). The system simplifies into a form for which surface temperature θ is a Lagrangian conserved tracer,

$$\frac{\partial \theta}{\partial t} + \mathbf{u} \cdot \nabla \theta = 0, \quad (2.3)$$

with \mathbf{u} defined as above and

$$\widehat{\theta} = -k \widehat{\psi} \quad (2.4)$$

(see Held *et al.* (1995) for details of the derivation). Here we considered the non-dimensional form of the equation so as to have a formal resemblance to (2.2).

Starting from these two models, it is possible to consider generalized models, where q is an active tracer obeying

$$\frac{\partial q}{\partial t} + \mathbf{u} \cdot \nabla q = 0 \quad (2.5)$$

and

$$\widehat{q} = -k^\alpha \widehat{\psi}, \quad (2.6)$$

with α a fixed parameter (Pierrehumbert *et al.* 1994). The case of $\alpha = 2$ corresponds to the QGBT model and $\alpha = 1$ gives the SQG model.

Such models possess generalized energies and enstrophies that are quadratic invariants. The generalized enstrophy expresses the variance of the scalar field q . Our interest will be focused on the cascade of this quantity to small scales. From heuristic arguments, its spectral flux η is set by $\eta \propto \sigma_k k \mathcal{Q}(k)$, where σ_k is the strain rate responsible for the stirring of the scalar at scale $1/k$ and $\mathcal{Q}(k)$ is the shell-averaged spectral density of generalized enstrophy. This last quantity is related to the global tracer variance through $Q = \langle q^2 \rangle = \int_0^\infty \mathcal{Q}(k) dk$, the angle brackets indicating an average over space. Assuming that σ_k depends only on the flow properties at the same local scale k and in the inertial range of the direct cascade of tracer variance, from $\eta = \text{const.}$ one obtains the (shell-averaged) kinetic energy spectrum

$$E(k) \propto \eta^{2/3} k^{-(4\alpha+1)/3} \quad (2.7)$$

for $\alpha < 2$ (Pierrehumbert *et al.* 1994), where $E(k)$ is related to the total kinetic energy \mathcal{E} through $\mathcal{E} = \int_0^\infty E(k) dk$. As the scaling law was obtained taking into account only local quantities (at scale k), this regime is associated with local transfers of generalized enstrophy. For $\alpha \geq 2$ the spectral flux no longer explicitly depends on the local wavenumber k , and

$$E(k) \propto \eta^{2/3} k^{1-2\alpha} \quad (2.8)$$

(Pierrehumbert *et al.* 1994; Watanabe & Iwayama 2004). This regime is associated with non-local generalized enstrophy transfers.

One important consequence of (2.7) is that the strain rate (responsible for the particle pair separation) between $1/k$ and $2/k$ behaves as $k^{2(2-\alpha)/3}$ for $\alpha < 2$. For these values of α , the exponent $2(2-\alpha)/3$ is positive and the dispersion of particles separated by a given distance should be controlled by eddies of comparable size. This would be associated with the ‘local dispersion’ regime. In contrast, for $\alpha \geq 2$, dispersion will be essentially governed by eddies at the largest scales, a regime corresponding to ‘non-local dispersion’. However, one should remember that the presence of nonlinear vortices generally tends to steepen the spectra, so that such phenomenological scalings are only an indication of what could be observed.

2.2. Relative dispersion

The dispersion of passive particles in a turbulent fluid has been widely studied and here we only present its main properties. The reader is referred to reviews by Falkovich *et al.* (2001), Sawford (2001), Bennett (2006) and Salazar & Collins (2009) for broader discussions.

Let us consider N particles whose positions at time t are denoted by $\mathbf{x}_i(t)$ with $i = 1, \dots, N$. Let us examine the pairs (i, j) satisfying $|\mathbf{x}_i(0) - \mathbf{x}_j(0)| = y_0$. Then relative dispersion is defined as

$$\langle y^2(t) \rangle = \langle |\mathbf{x}_i(t) - \mathbf{x}_j(t)|^2 \rangle, \quad (2.9)$$

where $\langle \rangle$ is the average over all of these pairs of particles. The vector $\mathbf{y}(t) = \mathbf{x}_i(t) - \mathbf{x}_j(t)$ is the separation vector between particles i and j , and $y^2 = |\mathbf{y}|^2$. From this, relative diffusivity can be computed as

$$K_{rel}(t) = \frac{1}{2} \frac{d\langle y^2(t) \rangle}{dt} = \langle \delta \mathbf{v}(t) \cdot \mathbf{y}(t) \rangle, \tag{2.10}$$

with the relative velocity defined by $\delta \mathbf{v}(t) = d\mathbf{x}_i/dt - d\mathbf{x}_j/dt = \mathbf{v}(\mathbf{x}_i(t), t) - \mathbf{v}(\mathbf{x}_j(t), t)$. Diffusivity can be rewritten as

$$\frac{1}{2} \frac{d\langle y^2(t) \rangle}{dt} = \langle \delta \mathbf{v}(t) \cdot \mathbf{y}_0 \rangle + \int_0^t \langle \delta \mathbf{v}(\tau) \cdot \delta \mathbf{v}(\tau) \rangle d\tau, \tag{2.11}$$

with $\mathbf{y}_0 = \mathbf{y}(t_0)$. Assuming that relative velocity is independent of the particle pair separation, i.e. $\langle \delta \mathbf{v}(t) \cdot \mathbf{y}_0 \rangle = 0$, for time sufficiently small one has

$$\langle y^2(t) \rangle \approx y_0^2 + \langle \delta \mathbf{v}_0 \cdot \delta \mathbf{v}_0 \rangle t^2, \tag{2.12}$$

with $\delta \mathbf{v}_0 = \delta \mathbf{v}(t=0)$. This result was obtained by Batchelor (1950) and was confirmed experimentally for 3D turbulent fluids by Bourgoïn *et al.* (2006) and Ouellette *et al.* (2006). This can be further simplified if one assumes that y_0 is sufficiently small and that velocity gradients are square-integrable. In that case, the structure function $S(y_0) = \langle \delta \mathbf{v}_0 \cdot \delta \mathbf{v}_0 \rangle$ can be replaced by Zy_0^2 , with $Z = \int_0^\infty k^2 E(k) dk$ the total relative enstrophy, and

$$\langle y^2 \rangle \approx y_0^2 (1 + Zt^2) \tag{2.13}$$

(Babiano *et al.* 1990). In the opposite limit of long times, one can expect that particles are separated by a distance larger than the largest eddies and, hence, relative diffusivity converges towards a constant that is twice the absolute diffusivity, due to uncorrelated particle velocities.

At intermediate times, for which dispersion scales are within the inertial range of the tracer variance cascade, the classical assumption of self-similarity for a local turbulent cascade can be made. In that case, diffusivity will depend only on η (the spectral turbulent flux of the tracer variance) and y (the distance of pair separation). The turbulent flux scales as $\eta = L^{4-2\alpha} T^{-3}$ (with L and T being typical length and time scales) and is assumed to be constant in the inertial range of the tracer variance cascade. We then obtain

$$\frac{1}{2} \frac{d\langle y^2 \rangle}{dt} \propto \eta^{1/3} \langle y^2 \rangle^{(\alpha+1)/3} \tag{2.14}$$

for $\alpha < 2$, which implies that

$$\langle y^2 \rangle \propto \eta^{1/(2-\alpha)} t^{3/(2-\alpha)}. \tag{2.15}$$

This is a generalization of Batchelor’s (1950) result for α -turbulence. Note that Morel & Larcheveque (1974) proposed another derivation based on the kinetic energy spectrum $E(k)$ and the dispersion scale. One can apply a hypothesis of local cascade using $(kE(k))^{1/2}/k$ as a diffusivity scale. By self-similarity and for a kinetic energy spectrum $E(k) \propto k^{-\beta}$, one can expect that

$$\frac{1}{2} \frac{d\langle y^2 \rangle}{dt} \propto \langle y^2 \rangle^{(\beta+1)/4}. \tag{2.16}$$

Relative dispersion then scales as

$$\langle y^2 \rangle \propto t^{4/(3-\beta)}. \quad (2.17)$$

Models with $0 < \alpha < 2$ satisfy $\beta = (4\alpha + 1)/3$, and (2.14) and (2.15) coincide with (2.16) and (2.17).

Fung & Vassilicos (1998) discuss the scaling relations obtained by the ‘locality hypothesis’ in their study of kinematic simulations of 2D flows possessing different energy spectra, while Nicolleau & Yu (2004) adopted a similar approach to examine the scalings in three dimensions. This latter study pointed out the necessity of taking into account finite scale effects due to the initial distance between particle pairs. This was also observed in previous studies dealing with direct numerical simulations of forced 2D turbulence (Babiano *et al.* 1990) and we will assess its importance in our simulations.

A different situation occurs when $\alpha \geq 2$, that is, for sufficiently steep ($\beta \geq 3$) kinetic energy spectra. In this case the flow is smooth and it can be shown that relative dispersion grows exponentially in time with an exponent related to the maximum Lagrangian Lyapunov exponent of the flow (Falkovich *et al.* 2001) or, equivalently, to the square root of enstrophy (LaCasce 2008):

$$\langle y^2 \rangle \propto e^{2c_1 Z^{1/2} t}, \quad (2.18)$$

where c_1 is a non-dimensional constant. Accordingly, one obtains

$$\frac{1}{2} \frac{d\langle y^2 \rangle}{dt} \propto c_1 Z^{1/2} \langle y^2 \rangle \quad (2.19)$$

for the relative diffusivity. This exponential growth of $\langle y^2 \rangle$ is essentially driven by the largest eddies and it does not depend on the slope of the kinetic energy spectrum. From a Lagrangian point of view this corresponds to a regime of ‘non-local dispersion’.

Table 1 summarizes the expected scalings from the type of α -model used (see §§ 5.2 and 5.3, respectively, for the definitions of FSLE and kurtosis). Note that these scalings do not contradict the initial ballistic regime (2.13) as discussed by Babiano *et al.* (1990) and Nicolleau & Yu (2004). One interpretation is that, as long as the separation vector does not reorient with respect to the spatial structure of the strain field (in particular the strain axes), the particle pairs retain memory of the initial velocity field, which leads to (2.13).

Equations (2.19) and (2.14) indicate that flows with non-local (respectively local) spectral transfers would imply non-local (respectively local) dispersion. However, the correspondence between transfers and dispersion properties breaks down if either the spectral transfers have both local and non-local contributions, or the energy spectra are steeper than predicted by the theory.

3. Numerical model

To explore in detail how local relative dispersion is in α -turbulence, we conduct simulations with different values of α ($= 1, 1.25, 1.5, 1.75, 2$). Two other simulations with very high viscosity are also performed with $\alpha = 1$ or $\alpha = 2$ in order to examine the relations between energy spectra and dispersion laws.

	$0 < \alpha < 2$	$\alpha \geq 2$
Kinetic energy spectral slope	$\beta = (4\alpha + 1)/3$	$\beta = 2\alpha - 1$
Relative dispersion	$\langle y^2(t) \rangle \propto t^{3/(2-\alpha)}$	$\langle y^2(t) \rangle \propto \exp(c_1 Z^{1/2} t)$
Diffusivity	$\frac{d\langle y^2 \rangle}{dt} \propto \langle y^2 \rangle^{(\alpha+1)/3}$	$\frac{d\langle y^2 \rangle}{dt} \propto \langle y^2 \rangle$
FSLE	$\lambda(\delta) \propto \delta^{2(\alpha-2)/3}$	$\lambda(\delta) \approx c_2$
Kurtosis	$ku(t) \approx c_3$	$ku(t) \propto \exp(c_4 t)$

TABLE 1. Scaling relations for relative dispersion indicators at intermediate scales as a function of α (see §§ 5.2 and 5.3, respectively, for the definitions of FSLE and kurtosis). The quantity Z is total relative enstrophy, and c_i ($i = 1$ to 4) are constants depending on properties of the fluid flow.

Equations (2.5) and (2.6) are integrated using a pseudo-spectral code with a fourth-order Runge–Kutta method for time stepping; an exponential filter provides numerical dissipation at small scales (LaCasce 1996). This filter allows extension of the inertial range of tracer variance flux over higher wavenumbers, compared to the usual hyperviscosity approach, with a very slow decay of energy in time (Smith *et al.* 2002). In the two viscous simulations, a standard Laplacian operator accounts for viscosity forces. Simulations are performed in free decay at a spatial resolution of 1024×1024 in a doubly periodic square box of side length 2π .

Despite the clear drawback due to their unsteady character, freely decaying runs can in the present case offer some advantages with respect to forced simulations. Indeed, these latter ones would necessitate determining what type of forcing to use, either correlated in space or time, random or deterministic, at large or small scales. Moreover, dissipation at large scales is also an important parameter since it can alter the cascade. As discussed by Burgess, Scott & Shepherd (2015), the kinetic energy spectral slope is sensitive to these choices and the values of these parameters. Also, one would need to decide which quantity will be kept constant between the different α cases: kinetic energy, generalized enstrophy or energy flux. We further remark that coherent eddies are affected by the forcing type, for instance, when using a random forcing on a particular wavenumber that will break the phase relationships of the vortices at this scale. This contrasts with freely decaying cases which allow the spontaneous emergence of coherent vortices. We leave for future investigation the case of forced simulations for which both direct and inverse cascades are resolved.

One difficulty in the present setting is to properly choose the initial condition for all the simulations so that the comparisons will be unbiased. Here all the simulations have been started with the same initial streamfunction, corresponding to Fourier components $\widehat{\psi}(\mathbf{k})$ satisfying

$$|\widehat{\psi}(\mathbf{k})|^2 = \frac{Ak^4}{(k + k_m)^{25}}, \quad (3.1)$$

with $k_m = 14$, and with random phases. This choice of k_m allows one to obtain a kinetic energy spectral peak at large scales, namely for $k = 7k_m/18 \approx 5.4$. The various simulations only differ in the amplitude of the initial streamfunction, as we choose to set the generalized energy equal to $\int k^\alpha |\widehat{\psi}|^2 d\mathbf{k} = 2 \times 10^{-3}$, which fixes the value of A for each experiment. In this way, we only affect the time scales of turbulence

and dispersion, and not the spatial scales of the stirring field (given by the relative enstrophy $k^2 E(k)$).

Concerning the computation of the trajectories of passive particles, we use the Lagrangian particle code used in Hua (1994), which calculates the velocity field at particle positions with a bicubic interpolation in space and integrates the trajectories in time with a fourth-order Runge–Kutta scheme. Such a scheme allows one to obtain robust statistics for relative dispersion (Zouari & Babiano 1990) and preserves the Lagrangian conservation of tracers (Hua 1994). We begin the integration of the particle trajectories at time $t = 40$ in dimensional units, when energy spectra of all simulations have reached an approximate equilibrium with distinct spectral slopes. The particles are set on a uniform grid and we checked that the initial velocity of particle separation is not correlated with the separation itself ($(\delta \mathbf{v}_0 \cdot \mathbf{y}_0) \approx 0$). Finally, we assume that particles move in an infinite domain and we use the periodicity of the fluid flow in physical space to compute their velocities when they leave the computational box.

4. Turbulent flow characteristics

4.1. Active tracer fields

After a transient period (that lasts until $t \approx 36$), the statistical properties of the different fields evolve more slowly with the continuous decay of the total energy (see supplementary material available at <https://doi.org/10.1017/jfm.2017.253> for more details about the quasi-steadiness of the turbulent regime). Figure 1 presents the active tracer fields for different values of α at $t = 40$. For $\alpha = 1$ (case of SQG turbulence), we observe intensified coherent structures from the smallest to the largest scales in the active tracer field q (figure 1*a*). These small-scale eddies are due to the instability of filaments that are expelled from larger-scale eddies (Held *et al.* 1995; Jukes 1995). This clearly also occurs in the case of $\alpha = 1.5$, e.g. for the filament with $q < 0$ that wraps up around the vortex at $(x, y) \approx (-2.2, -1.3)$ (figure 1*b*). Going to greater values of α , we observe the progressive disappearance of these small-scale eddies and the appearance of very long, thin and quasi-passive filaments (see figure 1*c* for $\alpha = 2$), as also observed by Pierrehumbert *et al.* (1994) in forced simulations. As discussed by Held *et al.* (1995), the decay range of the velocity field due to large-scale eddies is much shorter for SQG than for QGBT. Hence the straining processes that suppress the development of the filament instability are less efficient in SQG than in QGBT, which leads to the roll-up of small filaments to form small-scale vortices in SQG. For the viscous run with $\alpha = 1$, small-scale vortices completely disappear and only large-scale vortices with a few thick filaments remain (figure 1*d*).

4.2. Kinetic energy spectra

Figure 2(*a*) presents the kinetic energy spectra for the different simulations averaged over several realizations between times $t = 36$ and $t = 40$. At scales below $k = 10$, they share approximately the same shape with a maximum of kinetic energy around $k = 4$. From $k = 20$ to $k = 200$, to a good extent, we observe a constant spectral slope in each simulation for the non-viscous runs, while the spectrum rapidly falls off for the two viscous runs. For values of $\alpha < 2$, the actual slopes are close to the predictions based on local transfer arguments (see table 2). For the case of $\alpha = 2$ the kinetic energy spectrum is observed to be steeper than k^{-3} , probably due to numerical dissipation effects (Boffetta & Ecke 2012).

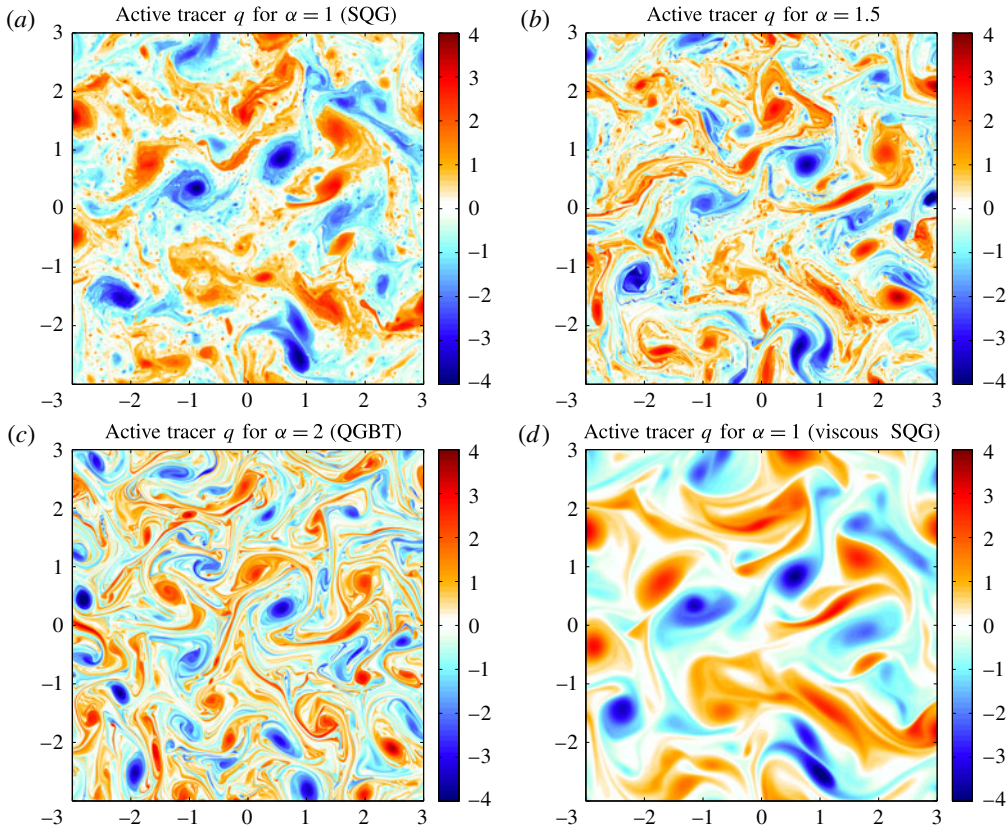


FIGURE 1. Active tracer q at $t=40$ for (a) $\alpha=1$, (b) $\alpha=1.5$, (c) $\alpha=2$ and (d) viscous run with $\alpha=1$. Values have been normalized by $\langle q^2 \rangle^{1/2}$ and the space domain is $[-\pi, \pi]^2$.

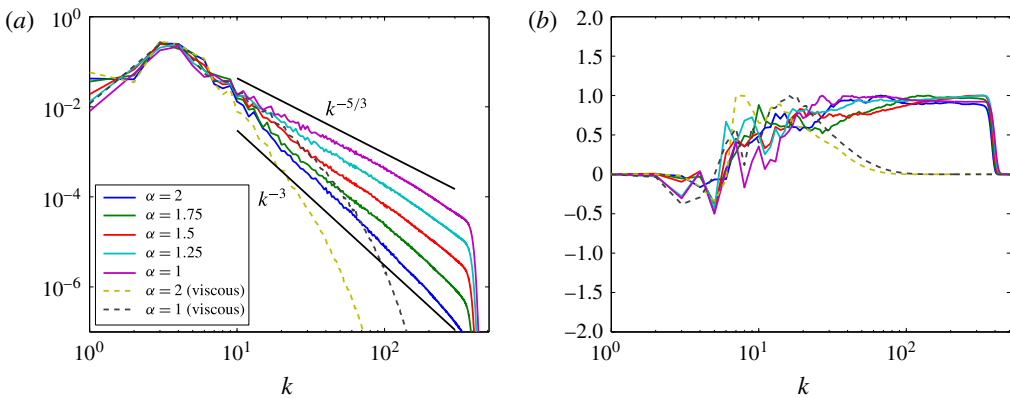


FIGURE 2. (a) Kinetic energy spectra normalized by total energy. (b) Spectral fluxes (normalized by their maximum value) of active tracer variance as a function of k . Spectra and fluxes have been time-averaged over several realizations between $t=36$ and $t=40$.

α	1	1.25	1.5	1.75	2
Theoretical slope	1.67	2	2.33	2.67	3
Observed slope	1.67	2.01	2.32	2.60	3.15

TABLE 2. Slopes of kinetic energy spectra ($E(k) \propto k^{-\beta}$) for different values of α , computed from a best fit in the range $20 \leq k \leq 200$. The uncertainties in the fitted values are of the order of 0.05. The theoretical slopes correspond to $\beta = (4\alpha + 1)/3$.

4.3. Spectral fluxes and non-locality

To further substantiate the existence of an inertial range with a corresponding direct cascade of active tracer q , we computed the tracer variance flux $\Pi(K)$ at each wavenumber K :

$$\Pi(K) = - \int_K^\infty [\text{Re}(\widehat{q}^*(\mathbf{u} \cdot \nabla q))] k dk, \tag{4.1}$$

where the square brackets indicate an average over time and over spectral shells around wavenumber modulus k . The notation $()^*$ stands for the complex conjugate and $\text{Re}()$ is the real part. Figure 2(b) presents the spectral flux $\Pi(K)$ for each case, normalized by its corresponding maximum value. In each simulation we observe that $\Pi(K) > 0$ for $8 < K < 300$, which confirms the existence of a direct cascade of active tracer q from large to small scales. Moreover, for most of the simulations, an inertial range (corresponding to constant flux) is found between approximately $K_{min}^i = 30$ and $K_{max}^i = 300$. For some α cases the plateaus of $\Pi(K)$ extend less towards the smaller wavenumbers. This might be the reason for the not exactly constant spectral slopes of the corresponding kinetic energy spectra at the lower boundary (in K) of the inertial range. The two viscous simulations do not possess any inertial range but still exhibit positive flux in a narrower range between $K \approx 8$ and $K \approx 80$. The absence of a constant energy flux range explains why there is no clear spectral slope for the kinetic energy spectrum (figure 2a).

To shed more light on the locality of transfers across scales, the tracer variance flux can be decomposed into transfers between modes. For a given wavenumber k , one can look for the scales (associated with wavenumbers l and m) that contribute to the flux at this scale. In such a situation, we have $k = l + m$. Such a combination of three scales corresponds to a triadic interaction (Kraichnan 1967).

A coarse-grained version of the tracer variance flux $T(n)$ for a circular shell $k_n < |\mathbf{k}| < k_{n+1}$ can be simply expressed as a triad transfer function from different scales:

$$T(n) = - \int_{k_n}^{k_{n+1}} [\text{Re}(\widehat{q}^*(\mathbf{u} \cdot \nabla q))] k dk = \sum_{a=0}^N \sum_{b=0}^N T(n|a, b), \tag{4.2}$$

where $T(n|a, b)$ represents the flux due to scales $l_a < |\mathbf{l}| < l_{a+1}$ and $m_b < |\mathbf{m}| < m_{b+1}$ (see Watanabe & Iwayama (2007) for more details). The full expression for $T(n|a, b)$ is given in appendix A.

The transfer function $T(n|a, b)$ is shown in figure 3 (for $n = 25$); here $k_n = \lambda^n$, $l_a = \lambda^a$, $m_b = \lambda^b$ and $\lambda = 1.2$. The index $n = 25$ corresponds to the shell centred on wavenumber 95, which is in the inertial range. For $\alpha = 2$ and $\alpha = 1.75$, we see that spectral transfers are due to triads with $a \ll b$ or $a \gg b$. This means that nonlinear transfers between triads are mostly non-local in these cases. While for $\alpha = 2$ this is

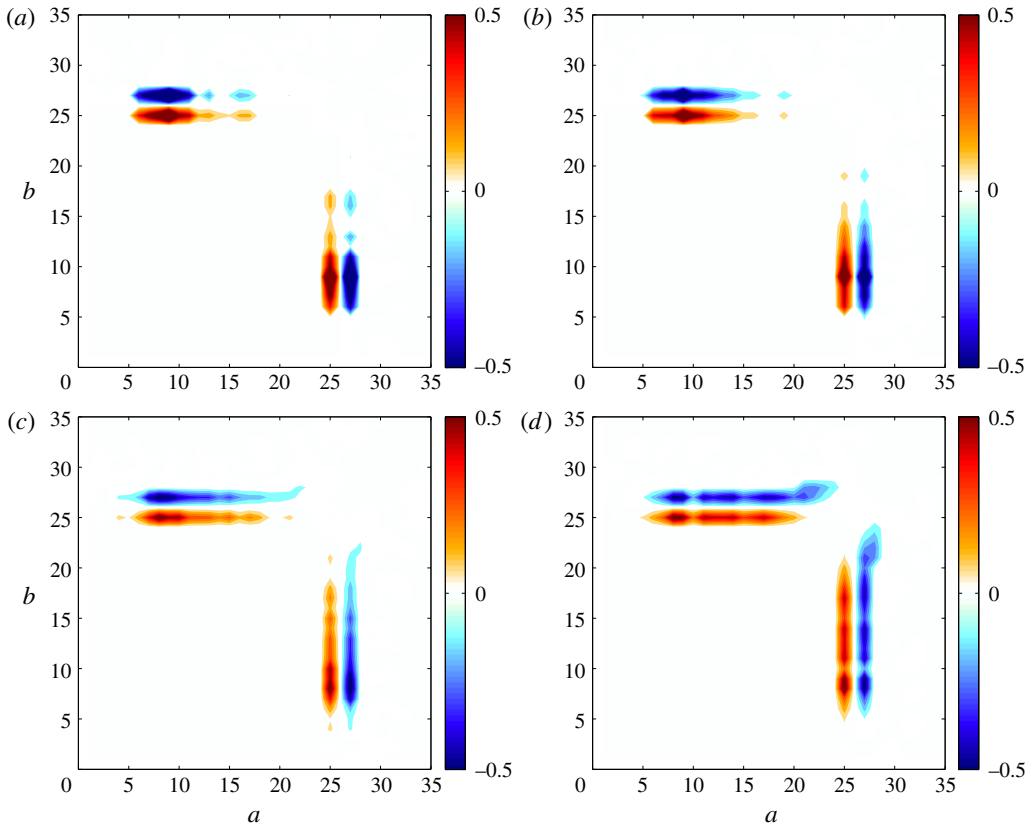


FIGURE 3. Coarse-grained triad transfer function $T(n|a, b)$ with $n = 25$ (corresponding to $k = 95$); the horizontal and vertical axes respectively correspond to the shell indices a and b . Cases with (a) $\alpha = 2$, (b) $\alpha = 1.75$, (c) $\alpha = 1.5$ and (d) $\alpha = 1$. Transfers have been time-averaged and normalized by the total tracer variance dissipation.

expected from the theory, this is less so when $\alpha = 1.75$. In contrast, for $\alpha = 1$ and $\alpha = 1.5$, triads with $a \approx b$ also contribute to the transfer function. In these two cases (in particular the SQG case), it has to be stressed that both local and non-local triads are responsible for the transfers while the phenomenological theory would advocate for only local contributions. Watanabe & Iwayama (2007) obtained the same results for the cases $\alpha = 1$ and $\alpha = 2$ in forced simulations. Hence, this result suggests that locality and non-locality in terms of turbulent energy transfers are not as exclusive as one might think *a priori*.

4.4. Locality of the strain field

The quantity that will matter in the dispersion of particles is the strain rate, as this governs the stirring of fluid parcels (see Lapeyre (2002) for a discussion on Lagrangian strain rates). A way to determine if a particular scale k will be strained by eddies of comparable size or by larger ones is to compute the weight of the strain rate at a given scale relative to the strain rate at larger scales. To this end we

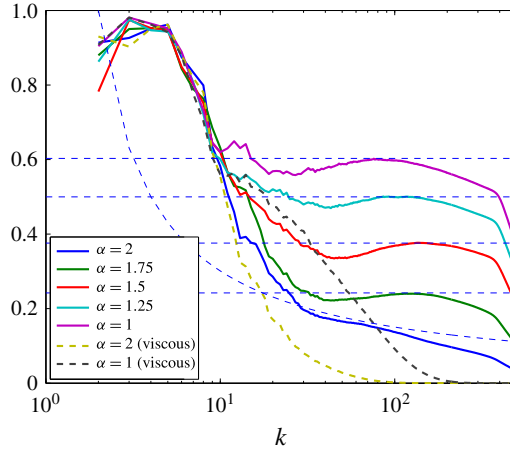


FIGURE 4. Ratio, R_k , of enstrophy contained in $[k/2, k]$ to enstrophy contained in $[k_{min}, k]$. The horizontal dashed curves correspond to the theoretical predictions R^{lim} , while the decreasing one is $R_k = \log 2 / \log(k/k_{min})$.

introduce the enstrophy ratio R_k :

$$R_k = \frac{\int_{k/2}^k l^2 E(l) dl}{\int_{k_{min}}^k l^2 E(l) dl}, \tag{4.3}$$

where the infrared cutoff $k_{min} > 0$ corresponds to the smallest wavenumber resolved in the domain, or the wavenumber containing the largest enstrophy at large scale. Here the numerator represents the local strain rate (more precisely the enstrophy $l^2 E(l)$) contained in eddies with size between $k/2$ and k , while the denominator expresses the strain rate by larger-scale structures felt by a given scale k (assuming that smaller-scale motions will not contribute to the stirring of larger-scale structures). Using a power-law spectrum $E(k) \sim k^{-(4\alpha+1)/3}$, the quantity R_k is equal to $R_k = (1 - 2^{4(\alpha-2)/3}) / (1 - (k_{min}/k)^{4(2-\alpha)/3})$ and tends to $R^{lim} = 1 - 2^{4(\alpha-2)/3}$ when k is large enough for $\alpha < 2$. For $\alpha = 2$, R_k decays as $R_k = \log 2 / \log(k/k_{min})$. Hence at large k , small eddies of size $1/k$ do not contribute to the stirring when $\alpha = 2$ whereas they have a non-negligible impact for $\alpha < 2$.

Figure 4 presents the quantity R_k along with its theoretical limit (dashed lines). At large scales, R_k is close to 1 for all cases, as can be understood from its definition in the limit of small wavenumbers. For smaller scales, namely those corresponding to $k > 30$, R_k decreases in fair agreement with the theoretical prediction for $\alpha = 2$, while it approaches a constant value for $\alpha < 2$. This value is close to $1 - 2^{4(\alpha-2)/3}$. As α decreases, local scales have a more and more important weight in the strain rate. However, R_k only reaches 60 % of the total strain for $\alpha = 1$. This indicates that larger scales still provide a non-negligible contribution to the stirring for the SQG case and raises the possibility that a dispersion theory based on local arguments might not be sufficient to account for the different processes involved in the dispersion.

5. Relative dispersion analysis

We now present the results of the relative dispersion analysis based on indicators computed both at fixed time and at fixed scale. For these calculations, an ensemble of 1024×1024 particles homogeneously distributed on a regular grid has been seeded in the flow after the transient regime, from time $t = 40$ to time $t = 80$. During this time interval, kinetic energy decayed by 17% or less (depending on the value of α), while the relative enstrophy decayed by almost 35% for all non-viscous runs (see supplementary material). During this time period, the relative enstrophy spectra keep the same shape for $k > 10$ while the main peak shifts to lower wavenumbers (not shown). Statistics were computed using up to 2×10^6 particle pairs. In the following, time $t = 0$ will correspond to the time of particle release.

5.1. Time-dependent statistics

As previous studies showed (Babiano *et al.* 1990; Boffetta & Sokolov 2002; Nicolleau & Yu 2004; Bourgoïn *et al.* 2006), relative dispersion statistics depend on the initial particle pair separation $y(t=0) = y_0$. It is then useful to introduce the wavenumber $k_0 = 2\pi/y_0$, which allows one to compare the initial pair separation with the typical length scales associated with the inertial range of the active tracer cascade. In the following we will take $k_0 = 512$, corresponding to initial separations $y_0 \approx 1.23 \times 10^{-2}$, smaller than the scale at which the tracer variance flux vanishes and the kinetic energy rapidly drops to zero, namely $k_v \approx 350$. We have also performed a particle release experiment with $k_0 = 1024$ but tracking particles over a more limited time period, and we obtained qualitatively similar results.

We further introduce a time scale corresponding to the time at which particle pairs have forgotten their initial separation, i.e. their early behaviour (see (2.12)). Such a time scale will take into account the period during which particles lose ‘memory’ of their initial position and velocities, which would delay the onset of scaling relations (see discussion in Babiano *et al.* 1990). For that purpose, we introduce a ‘memory index’,

$$M(t) = \frac{\langle \mathbf{y} \cdot \mathbf{y}_0 \rangle}{y_0 \langle y^2 \rangle^{1/2}}, \quad (5.1)$$

and we look for times t such that $M(t) \approx 0$. Figure 5 shows such a quantity in the case of $k_0 = 512$. Here, we rescaled time as $t_m = t/\tau_m$, where τ_m is such that $M(t = \tau_m) = 0.5$ for each value of α . We clearly observe that the separation distance decorrelates with its initial value in the same manner for all simulations, provided the appropriate time scale τ_m is used to make time non-dimensional. The cases $\alpha = 1$ and 1.25 seem to decorrelate more slowly in time but the difference with the other cases remains quite small. Hence, the time scale τ_m seems to provide the typical time scale of decorrelation with the initial conditions, and in the following we will use t_m as the rescaled time for an appropriate comparison of the different cases. We note that another time scale $T_z = Z^{-1/2}$, based on the relative enstrophy Z , could be appropriate. We found that this time scale is highly correlated with τ_m since the ratio T_z/τ_m stays between 0.5 and 0.8 for the different cases (not shown). However, t_m was found to give better agreement between the different simulations.

For short times ($t_m \ll 1$), we expect relation (2.12) to hold. Figure 6(a) clearly indicates that this regime is observed up to a time $t_m \approx 1$. This is in agreement with other studies (Nicolleau & Yu 2004; Bourgoïn *et al.* 2006). We note that simulations with different values of α and k_0 give exactly the same typical law $\langle y^2 \rangle \approx y_0^2(1 + ct_m^2)$ for sufficiently small t_m , with c a constant independent of α and k_0 – see the

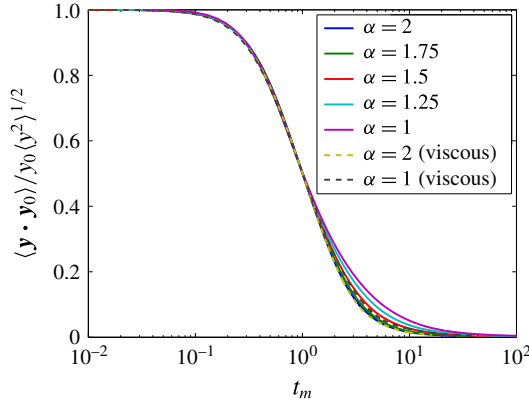


FIGURE 5. Particle separation memory index $M(t) = \langle \mathbf{y} \cdot \mathbf{y}_0 \rangle / y_0 \langle y^2 \rangle^{1/2}$ as a function of the renormalized time $t_m = t / \tau_m$. Initial pair separations correspond to $k_0 = 2\pi / y_0 = 512$.

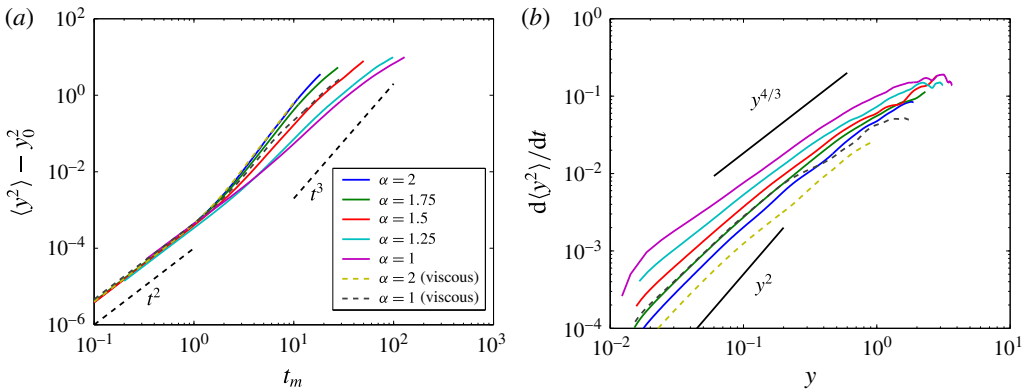


FIGURE 6. (a) Relative dispersion (after subtraction of the initial value) $\langle y^2 \rangle - y_0^2$ as a function of time t_m . (b) Diffusivity $d\langle y^2 \rangle / dt$ as a function of $\langle y^2 \rangle^{1/2}$. In this panel, only data with $M(t) < 0.5$ have been plotted. In each case, the initial separation y_0 corresponds to $k_0 = 512$.

good collapse of the different curves in figure 6(a) when varying α at fixed k_0 and figure 7 when varying k_0 at fixed α . This indicates that τ_m is the relevant time scale for comparing the different simulations. For each value of α the departure from the ballistic regime seems to occur around a common value between $t_m = 1$ and $t_m = 2$. At that time, the dispersion scale is of the order of $y^2 \approx (2\pi / K_{max}^i)^2 \approx 4.4 \times 10^{-4}$, i.e. in the inertial range.

We now turn to intermediate times for which the dispersion should obey a power law $\langle y^2 \rangle \propto t^{3/(2-\alpha)}$ for $\alpha < 2$ and an exponential law for $\alpha = 2$ and the viscous runs (table 1). Figure 6(a) shows that relative dispersion increases more rapidly when α increases, as expected. However, $\langle y^2 \rangle$ is systematically found to grow in time more slowly than predicted by the theory. A difficulty in measuring the power-law exponents (or exponential growth rates) is due to the fact that they strongly depend on k_0 , and they typically increase with it. Figure 7 displays $\langle y^2 \rangle / y_0^2$ as a function of time for different k_0 when $\alpha = 1$ (a) and $\alpha = 2$ (b). In both cases, we see that

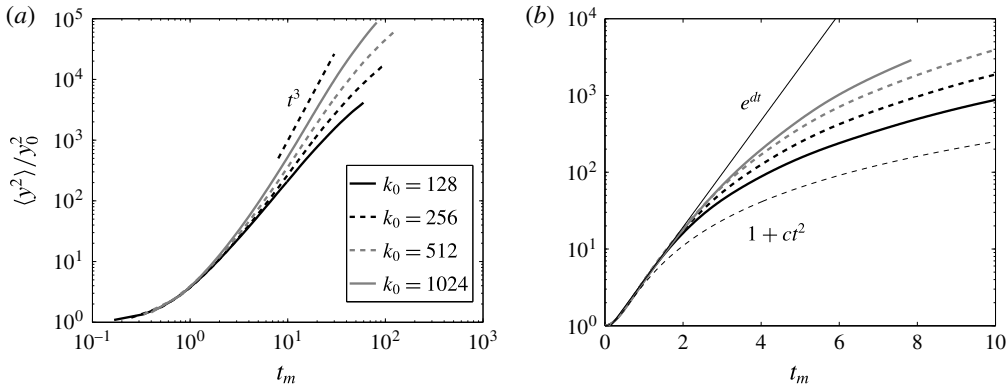


FIGURE 7. Relative dispersion as a function of time t_m for different values of y_0 (with $k_0 = 2\pi/y_0$) for $\alpha = 1$ (a) and $\alpha = 2$ (b). Here d is a constant proportional to the square root of relative enstrophy.

the asymptotic dispersion regime is better realized when increasing k_0 . For $\alpha = 1$ (figure 7a), relative dispersion tends to approach the theoretical expectation $\langle y^2 \rangle \sim t^3$ when y_0 is decreased, but the scaling is still limited to a quite short range even for the smallest y_0 considered. On the other hand, for $\alpha = 2$ (figure 7b), after a growth in $1 + ct_m^2$ up to $t_m \approx 1$, the time evolution of relative dispersion might suggest an exponential law, but only visible for smaller and smaller values of y_0 and up to a time $t_m \approx 2$. Such difficulties in observing clear scalings relating relative dispersion with time were noted by numerous authors (Morel & Larcheveque 1974; Boffetta & Sokolov 2002; Jullien 2003; Nicolleau & Yu 2004). Here two reasons can be invoked. Relative dispersion $\langle y^2 \rangle$ involves particle pairs with different histories: some may separate more slowly than others, e.g. if they are trapped inside coherent vortices. This can lead to spurious behaviours due to averaging together, at fixed time, potentially very different pair separations (Artale *et al.* 1997). Another possible reason lies in the weakly non-stationary character of the turbulent flow; indeed, relative enstrophy slowly decreases in time, causing a temporal variation of the exponential growth rate of the squared separation for $\alpha = 2$.

5.2. Scale-dependent statistics

Statistics at fixed scale are preferable to avoid the superposition of different dispersion regimes due to particle pairs having different histories (Morel & Larcheveque 1974; Bennett 1984; Aurell *et al.* 1997; LaCasce & Bower 2000).

Figure 6(b) shows relative diffusivity $d\langle y^2 \rangle/dt$ as a function of pair dispersion $y = \langle y^2 \rangle^{1/2}$ for an initial separation corresponding to $k_0 = 512$. Only data for which the particle pairs have forgotten their initial separation (i.e. $t > \tau_m$) have been plotted. The existence of a power-law regime appears more clearly when using this indicator. To better estimate the correspondence with the theory, a compensated plot $d\langle y^2 \rangle/dt \times \langle y^2 \rangle^{-(\alpha+1)/3}$ can be examined (figure 8). When decreasing the initial separation distance y_0 (or increasing k_0) for $\alpha < 2$, we see that a regime of quasi-constant compensated diffusivity (i.e. a broadening of the main peak) appears. This is more true when α is small and when k_0 is large. In particular, for $\alpha = 1$ and $\alpha = 1.25$ (figure 8a,b), we clearly see that the compensated diffusivity becomes constant over a large range of y . Note also that for the viscous case $\alpha = 2$, a restricted range of constant compensated

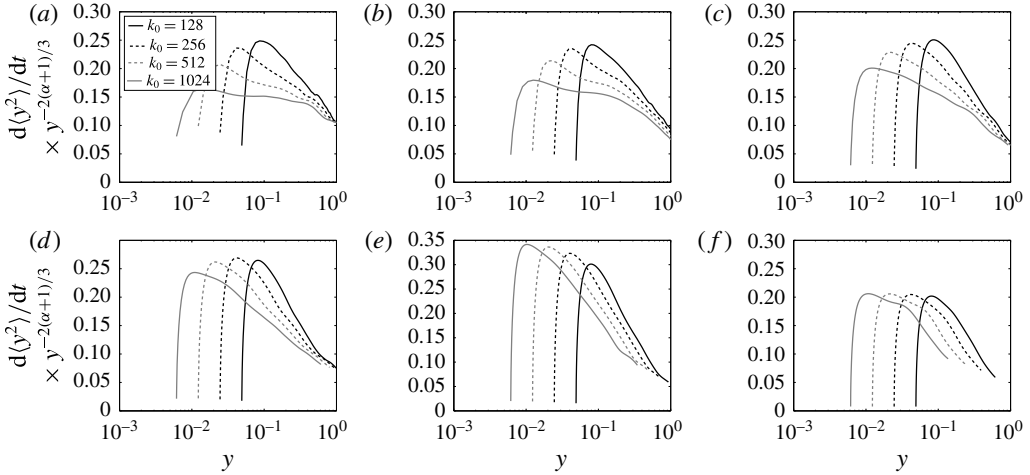


FIGURE 8. Compensated diffusivity $d\langle y^2 \rangle / dt \times \langle y^2 \rangle^{-(\alpha+1)/3}$ as a function of $\langle y^2 \rangle^{1/2}$. Panels (a–e) $\alpha = 1, 1.25, 1.5, 1.75, 2$. Panel (f) is the viscous case $\alpha = 2$. The different curves correspond to different values of initial separation distance.

diffusivity appears (figure 8f). For these different cases, we are confident that the dispersion statistics obey scaling laws predicted by the self-similarity theory based on a local cascade. However, this is only confirmed for small enough y_0 . For $\alpha = 2$, the compensated diffusivity does not show a clear plateau even for $k_0 = 1024$ (figure 8e). A similar conclusion is obtained for the viscous case $\alpha = 1$ (not shown).

With regard to the difficulty of observing exponential growth when $\alpha = 2$, an alternative diagnostic is the characteristic time of relative dispersion, defined in Babiano *et al.* (1990) as

$$\tau_{exp}(y) = \frac{\langle y^2 \rangle}{d\langle y^2 \rangle / dt}. \tag{5.2}$$

A constant value of $\tau_{exp}(y)$ corresponds to an exponential separation and defines the range of separations over which this regime is found. The behaviour of this quantity for different initial separations is presented in figure 9, again for $\alpha = 1, \alpha = 2$ and the viscous run with $\alpha = 2$. We have rescaled τ_{exp} with its minimum value in each case and only data in the inertial range are shown. For $\alpha = 1$, we do not expect an exponential regime and this serves to contrast with the other two cases. Indeed, in this case, the time scale τ_{exp} increases very rapidly with y (figure 9a), which indicates that an exponential growth is not present for the values of y_0 considered. For $\alpha = 2$ the characteristic time τ_{exp} is found to be constant, or at least to vary weakly (between 1 and 2) over a broader range of scales (almost a decade in y for the smallest y_0). This strongly suggests that non-local dispersion is taking place in the inertial range. As can be seen, the smaller the initial separation, the larger the range of separations for which $\tau_{exp}(y) = \text{const.}$, consistent with Babiano *et al.* (1990). In contrast to the $\alpha = 1$ case, the minimum of τ_{exp} was found to be independent of y_0 (not shown). The viscous run with $\alpha = 2$ reveals a much clearer exponential range, indicating that steeper energy spectra are accompanied by more non-local dispersion.

Another way to diagnose local/non-local dispersion is to investigate the exponential growth rate of separation, not as a function of time, but scale by scale. To this end, one can measure the time $\tau(\delta)$ needed to observe the growth of separation from a

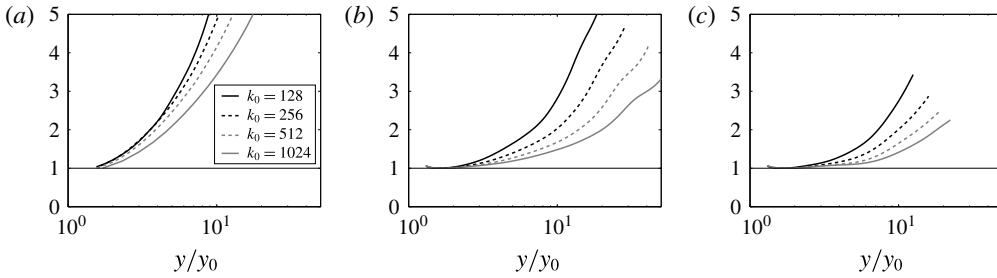


FIGURE 9. Characteristic time of relative dispersion τ_{exp} as a function of y/y_0 for $\alpha = 1$ (a), $\alpha = 2$ (b) and the viscous run with $\alpha = 2$ (c). Only data for which y is within the inertial range are displayed and $t_m > 1$. The value τ_{exp} has been rescaled by its minimum value. For $k_0 = 1024$ the inertial range occurs from $y/y_0 > 3.4$, while it is below 2 for the other values of k_0 .

scale δ to a scale $r\delta$ (with $r > 1$). The finite-size Lyapunov exponent (FSLE) is then defined as

$$\lambda(\delta) = \frac{\log(r)}{\langle \tau(\delta) \rangle}, \quad (5.3)$$

where the angular brackets indicate an average over all particle pairs (Artale *et al.* 1997; Aurell *et al.* 1997). If the kinetic energy spectrum scales as $k^{-\beta}$, the FSLE is expected to be given by

$$\lambda(\delta) \propto \delta^{(\beta-3)/2} \quad (5.4)$$

for $\beta < 3$. The power-law dependence as a function of α is then

$$\lambda(\delta) \propto \delta^{2(\alpha-2)/3} \quad (5.5)$$

when $\alpha < 2$. For spectra steeper than k^{-3} or for $\alpha \geq 2$, $\lambda(\delta)$ should reach a constant value. In such a case of scale-independent FSLE, dispersion is controlled by non-local processes, that is, by velocity field features at much larger scales than the particle separation. In the limit of infinitesimal separation, $\lambda(\delta)$ converges to the maximum Lagrangian Lyapunov exponent λ_L of the flow.

In our different simulations, the FSLE was computed using the scale separation factor $r = 1.2$, original pairs and the time of first crossing technique, but the results were qualitatively the same using chance pairs or the fastest crossing method (Lumpkin & Elipot 2010). Consistent with Özgökmen *et al.* (2012), we rescaled FSLE with the Okubo–Weiss parameter Q (Okubo 1970; Weiss 1991) that characterizes hyperbolic regions of the flow.

The behaviour of the FSLE is displayed in figure 10. For $0.03 < \delta < 0.3$, approximately corresponding to $20 < k < 200$, i.e. in the wavenumber range where constant spectral slopes were detected (see figure 2a), we observe a power law $\lambda(\delta) \propto \delta^{-\gamma}$ with an exponent γ that decreases as the slope of the kinetic energy spectrum increases (see table 3). This is in qualitative agreement with the theory but we remark that the decrease of $\lambda(\delta)$ with δ is slightly slower than expected for $\alpha = 1$ and $\alpha = 1.25$. At scales smaller than $\delta = 0.03$, $\lambda(\delta)$ displays some tendency to flatten in all cases, but no clear plateau region allowing the measurement of λ_L is detected, at least for $\alpha \leq 1.75$. The cases with $\alpha = 2$ and the two viscous runs present a considerably weaker scale dependence, with almost constant FSLE up to

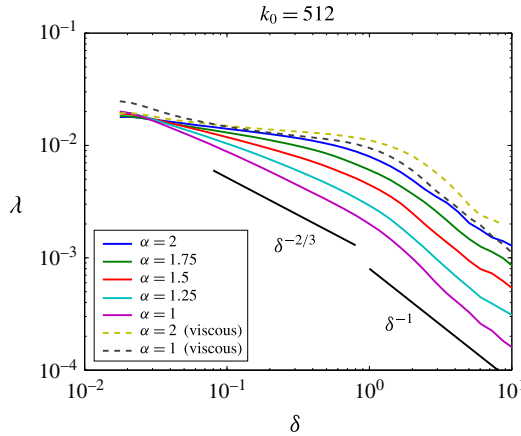


FIGURE 10. FSLE (rescaled by the Okubo–Weiss parameter) computed from original pairs with particles regularly spaced every $2\pi/512$ in each direction. Regimes $\lambda \propto \delta^{-2/3}$ and $\lambda \propto \delta^{-1}$ are indicated for comparison.

α	1	1.25	1.5	1.75	2	1 (viscous)	2 (viscous)
γ as in $\lambda(\delta) \propto \delta^{-\gamma}$	0.56	0.44	0.32	0.21	0.15	0.15	0.11
Theoretical value based on α	0.67	0.5	0.33	0.17	0	0	0

TABLE 3. Slopes of FSLE $\lambda(\delta)$ computed in the range $0.03 < \delta < 0.3$ (with uncertainties of the order of 0.05) and comparison with predictions based on α .

scales $\delta \approx 0.5$, pointing to an essentially non-local dispersion regime. Notice that the steepening of the FSLE for $\delta < 0.1$ for the viscous run with $\alpha = 1$ may be due to the fact that particles at small separation slowly forgot their initial separation. Finally, independently of the value of α , for $\delta > 1$ we observe a faster decrease with δ of the FSLE, but the behaviour of these scales $\delta > \pi$ may be misleading, as periodicity in the velocity field may modify the dispersion properties.

5.3. Higher-order statistics

Relative dispersion is the second-order moment of particle pair separation. While for Gaussian probability distributions knowledge of it provides a good characterization of the statistics, this is no longer true for strongly non-Gaussian distributions, such as those typically encountered in turbulence. In such a case it is useful to compute higher-order moments or the probability density function (p.d.f.) itself. As discussed in detail by Bennett (1984) and LaCasce (2010), the shapes of p.d.f.s give substantial information to determine what kind of dispersion regime is present.

In a 2D homogeneous incompressible flow the p.d.f. of pair separation $P(y, t)$ evolves according to the following Fokker–Planck equation (Richardson 1926):

$$\frac{\partial P}{\partial t} = \frac{1}{y} \frac{\partial}{\partial y} \left(y K_{rel} \frac{\partial P}{\partial y} \right), \tag{5.6}$$

where y is the pair separation (Bennett 1984; LaCasce 2010). Equation (5.6) must be supplemented by an initial condition such as, for example,

$$P(y, t = 0) = \frac{1}{2\pi y} \delta(y - y_0). \quad (5.7)$$

For a diffusivity $K_{rel} = \kappa y^a$ with $a < 2$, using the Laplace transform one can find the general solution

$$P(y, t) = \frac{1}{4\pi\kappa t (yy_0)^{a/2}} \exp\left(-\frac{1}{(a-2)^2} \frac{y^{2-a} + y_0^{2-a}}{\kappa t}\right) I_{a/(2-a)}\left(\frac{2}{(a-2)^2} \frac{(yy_0)^{1-a/2}}{\kappa t}\right), \quad (5.8)$$

where I_n is the modified Bessel function of order n . In the limit of large distances but before the final diffusive range ($y \gg y_0$ and $\kappa t \gg y^{2-a}$), one has

$$P(y, t) \approx \frac{1}{4\pi\Gamma(2/(2-a))((2-a)\kappa t)^{2/(2-a)}} \exp\left(-\frac{1}{(a-2)^2} \frac{y^{2-a}}{\kappa t}\right), \quad (5.9)$$

which is known as the Richardson p.d.f. for $a = 4/3$. In contrast, when $a = 2$, the law is log-normal, and it is known as the Lundgren p.d.f. (Lundgren 1981):

$$P(y, t) = \frac{1}{4\pi(\pi t/T)^{1/2} y_0^2} \exp\left(-\frac{[\ln(y/y_0) + 2t/T]^2}{4t/T}\right), \quad (5.10)$$

where the time scale T is proportional to the inverse cube root of the enstrophy dissipation rate (Lin 1972). Note that if one uses $K_{rel} = \kappa t^b$ instead of $K_{rel} = \kappa y^a$ in (5.6), a different p.d.f. can be obtained, in particular a Gaussian form in three dimensions for $b = 3$ (Batchelor 1952a). In 3D turbulent experiments, Ouellette *et al.* (2006) showed the dependence of the observed p.d.f. on the initial pair separations, which suggests that in particular cases (5.8) is preferable to (5.9) when comparing with observations.

Figure 11 presents the p.d.f. observed at different times, and with $k_0 = 2\pi/y_0 = 512$, for the two extreme cases (a) $\alpha = 2$ (QGBT) and (b) $\alpha = 1$ (SQG) corresponding to $a = 2$ and $a = 4/3$, respectively.

Figure 11(a) indicates that the case $\alpha = 2$ is representative of a Lundgren law, at least for $t_m \leq 10$. Note that the correction $2t/T$ in (5.10) was found to be small. The adequacy of the Lundgren law in representing the dispersion p.d.f. provides strong support for non-local dispersion, in a more unambiguous way than the dispersion, diffusivity or FSLE. For larger times and y much larger than its initial value, the p.d.f. is less well approximated by this law. This particularly occurs for the right tail of the p.d.f. even at $t_m > 6$ and is in agreement with the fact that at such times the exponential dispersion law is not observed (figure 7b). In the case $\alpha = 1$ (figure 11b), the separation p.d.f. substantially differs from the Lundgren solution compared to the other case but is reasonably well captured by the prediction of (5.9) with $a = 4/3$, corresponding to a Richardson distribution, in the range $6.5 \leq t_m \leq 25$. The strong fluctuations of the p.d.f.s visible in figure 11(a,b) for $y < y_0$ are due to limited statistics at very small separations.

The p.d.f. allows one to compute all moments such as, for example, relative dispersion. Interesting information is also provided by the kurtosis of relative

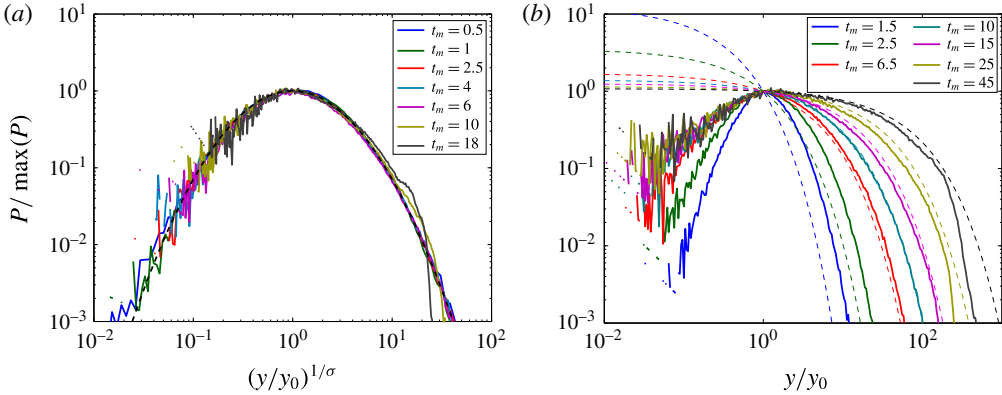


FIGURE 11. Probability density functions of pair separations for (a) $\alpha = 2$ and (b) $\alpha = 1$ at different values of t_m . In panel (a), the p.d.f.s are shown as a function of the rescaled variable $(y/y_0)^{1/\sigma} = \exp[(1/\sigma)(\log y - \log y_0)]$, where σ is the standard deviation of the p.d.f. in log space. The Lundgren distribution is represented by the black dashed curve. In panel (b), the p.d.f.s are shown as a function of y/y_0 . The dashed lines correspond to the Richardson solutions. In all cases the initial separation of particle pairs corresponds to $k_0 = 512$.

displacements, which samples the high tails of the distribution corresponding to rare and very large particle separations. It is defined as

$$ku(t) = \frac{\langle y^4 \rangle}{\langle y^2 \rangle^2}. \quad (5.11)$$

For a Rayleigh distribution (the expected one for a normally distributed random process and in the diffusive limit of dispersion), $ku = 2$ (LaCasce 2010). In the Richardson regime, the kurtosis would attain a value close to 5.6, while it would exponentially grow in time in the (marginally) non-local regime of the enstrophy cascade (associated with exponential growth of relative dispersion) as shown by LaCasce (2010).

Figure 12 presents the time evolution of kurtosis for initial particle separations corresponding to $k_0 = 512$. There is a clear difference between simulations with $\alpha \geq 1.75$ or the viscous ones, whose kurtosis reaches values larger than 15, and simulations with $\alpha \leq 1.5$, whose kurtosis does not exceed 12 and is not so prominently peaked. The behaviour for $\alpha = 2$ and the viscous runs is in reasonable agreement with an exponential growth of separation and a dispersion process driven by large scales (LaCasce 2008) and seems to be in agreement with the FSLE.

6. Conclusions

We examined a class of generalized 2D turbulent flows (α -turbulence models), encompassing the QGBT and SQG models as limiting cases (Pierrehumbert *et al.* 1994). All of these models have dynamics characterized by the conservation of an active tracer along the geostrophic flow with a direct cascade of tracer variance to small scales. As expected, the numerically computed kinetic energy spectral slopes are close to the predictions based on phenomenological arguments for $1 \leq \alpha < 2$, while the spectrum was found to be quite steep in our simulations for $\alpha = 2$ (probably

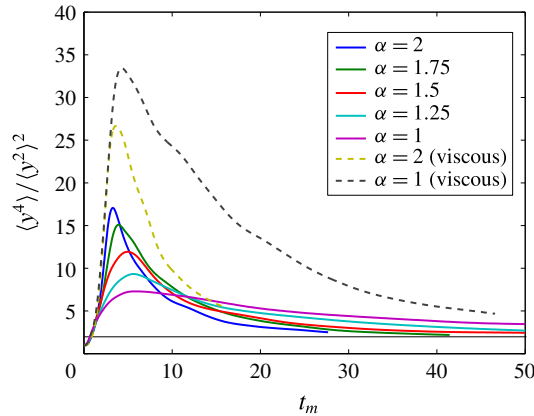


FIGURE 12. Relative displacement kurtosis as a function of t_m ; here $k_0 = 512$. The black thin line corresponds to a kurtosis of $\langle y^4 \rangle / \langle y^2 \rangle^2 = 2$ (representative of a Rayleigh distribution).

due to numerical dissipation effects) and the two viscous runs. We examined the spectral transfers of active tracer variance between scales and found that both local and non-local triads contribute to the transfers, contrary to the general phenomenology assumption.

We further analysed relative dispersion statistics both as a function of time and as a function of scale in order to see how the phenomenological scaling laws predicted by local self-similarity arguments were verified. As in previous studies, we found that the scalings of relative dispersion as a function of time are difficult to assess, due to the strong dependence on initial pair separations. In particular, the exponential growth of relative dispersion in the case of $\alpha = 2$ was observed for a limited range of time, even for initial separations much smaller than the inertial range scales. In that respect, different fixed-scale statistical indicators were able to reveal this exponential growth. For $1 \leq \alpha < 2$, relative dispersion was found to follow the power laws expected from local cascade theories. This is more true when α is close to 1 and the initial pair separation is small. Finally, the relative displacement p.d.f.s were consistent with a Lundgren distribution for $\alpha = 2$ and a Richardson distribution for $\alpha = 1$.

This study has provided evidence that relative dispersion in SQG turbulent flows ($\alpha = 1$) is local, in the sense that small-scale eddies govern relative dispersion at their scale, while in QGBT flows ($\alpha = 2$) dispersion is governed by large-scale eddies (non-local dispersion). Hence large-scale eddies have little effect on the dispersion in SQG flows when considering small enough separations. An unexpected element is that, for the SQG case and more generally for $\alpha < 2$, spectral transfers of the active tracer variance between scales have both local and non-local components, i.e. modes associated with very different wavenumbers do contribute to the transfer. Hence, the concept of local/non-local interactions in the cascade of an active scalar does not seem to be straightforwardly related to that of locality of particle dispersion. In our opinion, what matters for the dispersion of particles is the self-similar character of the turbulent dynamics, which determines both the spectral behaviour of the flow and the dispersion laws.

This result was obtained in the context of freely decaying simulations with a kinetic energy peak at large scale. It would be interesting to examine the case of

forced simulations with the simultaneous presence of both a direct and an inverse cascade. Another interesting question would be to compare the dispersion in different α -turbulence models having the same kinetic energy spectrum but different cascade directions. In this class of models, the QGBT inverse cascade has a typical $k^{-5/3}$ law for the kinetic energy spectrum, which is similar to the kinetic energy spectrum of the SQG direct cascade. Comparing models with similar kinetic energy spectral slopes would allow one to assess the different features of the turbulent dynamics that determine the relative dispersion characteristics.

Acknowledgements

We thank anonymous reviewers who helped to improve the manuscript with their constructive comments. X.P. acknowledges the funding support of ANR ASIV (ANR-11-Blanc-5-6-014). This work is a contribution to the SWOT project and was supported by TOSCA/CNES.

Supplementary material

Supplementary material is available at <https://doi.org/10.1017/jfm.2017.253>.

Appendix A. Coarse-grained transfer function

The transfer of tracer variance towards wavevector \mathbf{k} is simply expressed as

$$-\text{Re}(\widehat{q}_k^* (\mathbf{u} \cdot \nabla q)_k). \quad (\text{A } 1)$$

This can be further expanded if we introduce wavevectors \mathbf{l} and \mathbf{m} as

$$-\text{Re} \left(\widehat{q}_k^* \sum_{\mathbf{l}+\mathbf{m}=\mathbf{k}} (\mathbf{u}_l \cdot \nabla q_m) \right), \quad (\text{A } 2)$$

where \mathbf{u}_l is the component of the velocity corresponding only to the wavevector \mathbf{l} and q_m is the tracer component corresponding to wavevector \mathbf{m} .

Let us now subdivide the wavenumber space into circular shells $k_0 < \dots < k_n < k_{n+1} < \dots < k_N$, $l_0 < \dots < l_a < l_{a+1} < \dots < l_N$ and $m_0 < \dots < m_b < m_{b+1} < \dots < m_N$. The contribution to the flux for the shell $k_n < k < k_{n+1}$ (see (4.2)) can be decomposed into individual transfers:

$$T(n|a, b) = - \sum_{k_n < |\mathbf{k}| < k_{n+1}} \sum_{l_a < |\mathbf{l}| < l_{a+1}} \sum_{m_b < |\mathbf{m}| < m_{b+1}} \delta_{k=|\mathbf{l}+\mathbf{m}|} \times \text{Re} \left(\widehat{q}_{n,n+1}^* [(\mathbf{u}_{a,a+1} \cdot \nabla q_{b,b+1}) + (\mathbf{u}_{b,b+1} \cdot \nabla q_{a,a+1})] \right), \quad (\text{A } 3)$$

with $F_{x,x+1}$ being the restriction of F to the shell with $k_x < |\mathbf{k}| < k_{x+1}$ and δ the Kronecker symbol. In (A 3), the quantity $T(n|a, b)$ represents the transfer of tracer variance from shells $l_a < l < l_{a+1}$ and $m_b < m < m_{b+1}$ to shell $k_n < k < k_{n+1}$.

REFERENCES

- ARTALE, V., BOFFETTA, G., CELANI, A., CENCINI, M. & VULPIANI, A. 1997 Dispersion of passive tracers in closed basins: beyond the diffusion coefficient. *Phys. Fluids A* **9**, 3162–3171.
- AURELL, E., BOFFETTA, G., CRISANTI, A., PALADIN, G. & VULPIANI, A. 1997 Predictability in the large: an extension of the concept of Lyapunov exponent. *J. Phys. A* **30**, 1–26.

- BABIANO, A., BASDEVANT, C., ROY, P. L. & SADOURNY, R. 1990 Relative dispersion in two-dimensional turbulence. *J. Fluid Mech.* **214**, 535–557.
- BATCHELOR, G. K. 1950 The application of the similarity theory of turbulence to atmospheric diffusion. *Q. J. R. Meteorol. Soc.* **551**, 133–146.
- BATCHELOR, G. K. 1952a Diffusion in a field of homogeneous turbulence II. The relative motion of particles. *Proc. Camb. Phil. Soc.* **48**, 345–362.
- BATCHELOR, G. K. 1952b The effect of homogeneous turbulence on material lines and surfaces. *Proc. R. Soc. Lond. A* **213**, 349–366.
- BENNETT, A. 2006 *Lagrangian Fluid Dynamics*. Cambridge University Press.
- BENNETT, A. F. 1984 Relative dispersion: local and nonlocal dynamics. *J. Atmos. Sci.* **41**, 1881–1886.
- BERTI, S. & LAPEYRE, G. 2014 Lagrangian reconstructions of temperature and velocity in a model of surface ocean turbulence. *Ocean Model.* **76**, 59–71.
- BERTI, S., DOS SANTOS, F., LACORATA, G. & VULPIANI, A. 2011 Lagrangian drifter dispersion in the Southwestern Atlantic Ocean. *J. Phys. Oceanogr.* **41**, 1659–1672.
- BOFFETTA, G. & CELANI, A. 2000 Pair dispersion in turbulence. *Physica A* **280**, 1–9.
- BOFFETTA, G. & ECKE, R. E. 2012 Two-dimensional turbulence. *Annu. Rev. Fluid Mech.* **44**, 427–451.
- BOFFETTA, G. & SOKOLOV, I. M. 2002 Statistics of two-particle dispersion in two-dimensional turbulence. *Phys. Fluids* **14**, 3224–3232.
- BOURGOIN, M., OUELLETTE, N. T., XU, H., BERG, J. & BODENSCHATZ, E. 2006 The role of pair dispersion in turbulent flow. *Science* **311**, 835–838.
- BURGESS, B. H., SCOTT, R. K. & SHEPHERD, T. G. 2015 Kraichnan–Leith–Batchelor similarity theory and two-dimensional inverse cascades. *J. Fluid Mech.* **767**, 467–496.
- ER-EL, J. & PESKIN, R. L. 1981 Relative diffusion of constant-level balloons in the Southern Hemisphere. *J. Atmos. Sci.* **38**, 2264–2274.
- FALKOVICH, G., GAWEDZKI, K. & VERGASSOLA, M. 2001 Particles and fluids in turbulence. *Rev. Mod. Phys.* **73**, 913–975.
- FUNG, J. C. H. & VASSILICOS, J. C. 1998 Two-particle dispersion in turbulentlike flows. *Phys. Rev. E* **57**, 1677–1690.
- GARRETT, C. 1983 On the initial streakiness of a dispersing tracer in two- and three-dimensional turbulence. *Dyn. Atmos. Oceans* **7**, 265–277.
- GRAFF, L. S., GUTTU, S. & LACASCE, J. H. 2015 Relative dispersion in the atmosphere from reanalysis winds. *J. Atmos. Sci.* **72**, 2769–2785.
- HELD, I. M., PIERREHUMBERT, R. T., GARNER, S. T. & SWANSON, K. L. 1995 Surface quasi-geostrophic dynamics. *J. Fluid Mech.* **282**, 1–20.
- HUA, B. L. 1994 The conservation of potential vorticity along Lagrangian trajectories in simulations of eddy-driven flows. *J. Phys. Oceanogr.* **24**, 498–508.
- HUA, B. L., MCWILLIAMS, J. C. & KLEIN, P. 1998 Lagrangian accelerations in geostrophic turbulence. *J. Fluid Mech.* **366**, 87–108.
- JUCKES, M. 1995 Instability of surface and upper-tropospheric shear lines. *J. Atmos. Sci.* **52**, 3247–3262.
- JULLIEN, M.-C. 2003 Dispersion of passive tracers in the direct enstrophy cascade: experimental observations. *Phys. Fluids* **15**, 2228–2237.
- JULLIEN, M.-C., PARET, J. & TABELING, P. 1999 Richardson pair dispersion in two-dimensional turbulence. *Phys. Rev. Lett.* **82**, 2872–2875.
- KLEIN, P., HUA, B. L. & LAPEYRE, G. 2000 Alignment of tracer gradient vectors in 2D turbulence. *Physica D* **146**, 246–260.
- KLEIN, P., LAPEYRE, G., ROULLET, G., LE GENTIL, S. & SASAKI, H. 2011 Ocean turbulence at meso and submesoscales: connection between surface and interior dynamics. *Geophys. Astrophys. Fluid Dyn.* **105**, 421–437.
- KOSZALKA, I., LACASCE, J. H. & ORVIK, K. A. 2009 Relative dispersion in the Nordic Seas. *J. Mar. Res.* **67**, 411–433.
- KOWALSKI, A. D. & PESKINS, R. L. 1981 Numerical simulation of relative dispersion in two-dimensional, homogeneous, decaying turbulence. *J. Fluid Mech.* **109**, 45–61.

- KRAICHNAN, R. H. 1967 Inertial ranges in two-dimensional turbulence. *Phys. Fluids* **10**, 1417–1423.
- LACASCE, J. H. 1996 Baroclinic vortices over a sloping bottom. PhD thesis, MIT/WHOI Joint Program in Physical Oceanography, p. 216.
- LACASCE, J. H. 2008 Statistics from Lagrangian observations. *Prog. Oceanogr.* **77**, 1–29.
- LACASCE, J. H. 2010 Relative displacement probability distribution functions from balloons and drifters. *J. Mar. Res.* **68**, 433–457.
- LACASCE, J. H. & BOWER, A. 2000 Relative dispersion in the subsurface North Atlantic. *J. Mar. Res.* **58**, 863–894.
- LACASCE, J. H. & OHLMANN, C. 2003 Relative dispersion at the surface of the Gulf of Mexico. *J. Mar. Res.* **61**, 285–312.
- LACORATA, G., AURELL, E., LEGRAS, B. & VULPIANI, A. 2004 Evidence for a $k^{-5/3}$ spectrum from the EOLE Lagrangian balloons in the low stratosphere. *J. Atmos. Sci.* **61**, 2936–2942.
- LAPEYRE, G. 2002 Characterization of finite-time Lyapunov exponents and vectors in two-dimensional turbulence. *Chaos* **12**, 688–698.
- LAPEYRE, G. 2017 Surface quasi-geostrophy. *Fluids* **2**, 7.
- LIN, J.-T. 1972 Relative dispersion in the enstrophy cascading inertial range of homogeneous two-dimensional turbulence. *J. Atmos. Sci.* **29**, 394–396.
- LUMPKIN, R. & ELIPOT, S. 2010 Surface drifter pair spreading in the North Atlantic. *J. Geophys. Res.* **115**, C12017.
- LUNDGREN, T. S. 1981 Turbulent pair dispersion and scalar diffusion. *J. Fluid Mech.* **111**, 27–57.
- MOREL, P. & LARCHEVEQUE, M. 1974 Relative dispersion of constant-level balloons in the 200-mb general circulation. *J. Atmos. Sci.* **31**, 2189–2196.
- NICOLLEAU, F. & YU, G. 2004 Two-particle diffusion and locality assumption. *Phys. Fluids* **16**, 2309–2321.
- OETZEL, K. G. & VALLIS, G. F. 1997 Strain, vortices and the enstrophy range in two-dimensional turbulence. *Phys. Fluids A* **9**, 2991–3004.
- OHKITANI, K. 1990 Nonlocality in a forced two-dimensional turbulence. *Phys. Fluids A* **2**, 1529–1531.
- OKUBO, A. 1970 Horizontal dispersion of floatable particles in the vicinity of velocity singularity such as convergences. *Deep-Sea Res.* **17**, 445–454.
- OLLITRAULT, M., GABILLET, C. & COLIN DE VERDIÈRE, A. 2005 Open ocean regimes of relative dispersion. *J. Fluid Mech.* **533**, 381–407.
- OUELLETTE, N. T., XU, H., BOURGOIN, M. & BODENSCHAT, E. 2006 An experimental study of turbulent relative dispersion models. *New J. Phys.* **8**, 109.
- ÖZGÖKMEN, T. M., POJE, A. C., FISCHER, P. F., CHILDS, H., KRISHNAN, H., GARTH, C., HAZA, A. C. & RYAN, E. 2012 On multi-scale dispersion under the influence of surface mixed layer instabilities and deep flows. *Ocean Model.* **56**, 16–30.
- PIERREHUMBERT, R. T., HELD, I. M. & SWANSON, K. L. 1994 Spectra of local and nonlocal two-dimensional turbulence. *Chaos, Solitons Fractals* **4**, 1111–1116.
- POJE, A. C., HAZAB, A. C., ÖZGÖKMEN, T. M., MAGALDI, M. G. & GARRAFFO, Z. D. 2010 Resolution dependent relative dispersion statistics in a hierarchy of ocean models. *Ocean Model.* **31**, 36–50.
- RICHARDSON, L. F. 1926 Atmospheric diffusion on a distance-neighbour graph. *Proc. R. Soc. Lond. A* **110**, 709–737.
- RIVERA, M. K. & ECKE, R. E. 2005 Pair dispersion and doubling time statistics in two-dimensional turbulence. *Phys. Rev. Lett.* **95**, 194503.
- SALAZAR, J. P. L. C. & COLLINS, L. R. 2009 Two-particle dispersion in isotropic turbulent flows. *Annu. Rev. Fluid Mech.* **41**, 405–432.
- SAWFORD, B. 2001 Turbulent relative dispersion. *Annu. Rev. Fluid Mech.* **33**, 289–317.
- SCHROEDER, K., CHIGGIATO, J., HAZA, A. C., GRIFFA, A., ÖZGÖKMEN, T. M., ZANASCA, P., MOLCARD, A., BORGHINI, M., POULAIN, P. M., GERIN, R. *et al.* 2012 Targeted Lagrangian sampling of submesoscale dispersion at a coastal frontal zone. *Geophys. Res. Lett.* **39**, 1168.
- SMITH, K. S., BOCCALETTI, G., HENNING, C. C., MARINOV, I. N., TAM, C. Y., HELD, I. M. & VALLIS, G. K. 2002 Turbulent diffusion in the geostrophic inverse cascade. *J. Fluid Mech.* **469**, 14–47.

- THOMSON, D. J. & DEVENISH, B. J. 2005 Particle pair separation in kinematic simulations. *J. Fluid Mech.* **526**, 277–302.
- VON KAMEKE, A., HUHN, F., FERNÁNDEZ-GARCÍA, G., MUÑUZURI, A. P. & PÉREZ-MUÑUZURI, V. 2011 Double cascade turbulence and Richardson dispersion in a horizontal fluid flow induced by Faraday waves. *Phys. Rev. Lett.* **107**, 074502.
- WATANABE, T. & IWAYAMA, T. 2004 Unified scaling theory for local and non-local transfers in generalized two-dimensional turbulence. *J. Phys. Soc. Japan* **73**, 3319–3330.
- WATANABE, T. & IWAYAMA, T. 2007 Interacting scales and triad enstrophy transfers in generalized two-dimensional turbulence. *Phys. Rev. E* **76**, 046303.
- WEISS, J. 1991 The dynamics of enstrophy transfer in two-dimensional hydrodynamics. *Physica D* **48**, 273–294.
- ZOUARI, N. & BABIANO, A. 1990 Expériences numériques lagrangiennes à partir de modèles eulériens. *Atmos.-Ocean* **28**, 345–364.